SAND2011-1915C

Mapping of 1D Beam Loads to the 3D Wind Blade for Buckling Analysis

Jonathan C. Berg[*], Joshua A. Paquette[†], Brian R. Resor[‡]
Sandia National Laboratories[§], Albuquerque, NM, 87185-1124

This paper discusses the development of a consistent methodology for mapping one-dimensional distributed beam loads to a three-dimensional shell structure. The resultant force distribution is a linear approximation to the actual aerodynamic pressure distribution but is sufficient to obtain accurate strain and displacement results. The purpose of the mapping technique is to apply more realistic wind loads to the shell model of a wind turbine blade without the need to set up and run expensive computational fluid dynamics or fluid structure interaction problems. Subsequent buckling and stress analysis reveal how this approach compares to other simplified methods of defining the loads.

Nomenclature

$f_{x,i}$ = *X* component of the force applied to node *i* of finite element shell model
$f_{y,i}$ = *Y* component of the force applied to node *i* of finite element shell model
F_x = *X* component of force reduced down from distributed pressure load
F_y = *Y* component of force reduced down from distributed pressure load
M = moment resulting from distributed pressure load
x_i = *x*-coordinate of finite element node *i*
y_i = *y*-coordinate of finite element node *i*

I. Introduction

Buckling load of wind turbine blade panels is an important design load case in the process of wind blade design. The reader is directed to Ref. 1 for a general introduction to buckling of shell structures and Ref. 2 for an example of the blade design process. Although the majority of the bending load is carried by the spar cap and shear web, the blade designer must also be concerned with panel buckling that can result when loading the blade skin in compression. The buckling analysis is often performed using a finite element (FE) shell model of the wind turbine blade. Appropriate loads must be applied to the nodes of the finite element model.

It is desirable to use the actual aerodynamic force distribution when performing the buckling analysis. As demonstrated in Ref. 3, pressure distributions obtained from CFD (Computational Fluid Dynamics) may be used effectively in buckling analysis. However, the blade designer often uses an aeroelastic model of the wind blade which has been reduced down to a simple beam model for computational efficiency. The aerodynamic loading typically consists of two forces and a moment applied at the center of each beam element in the one-dimensional beam. Although these forces may be applied as point loads to the FE mesh, a more realistic and consistent approach distributes the forces among all FE nodes while maintaining the overall equivalent force and moment distribution imparted by the aeroelastic model.

[*] Member of the Technical Staff, Wind & Water Power Technologies, P.O. Box 5800
[†] Senior Member of the Technical Staff, Wind & Water Power Technologies, P.O. Box 5800
[‡] Senior Member of the Technical Staff, Wind & Water Power Technologies, P.O. Box 5800
[§] Sandia is a multiprogram laboratory operated by Sandia Corporation, a Lockheed Martin Company, for the United States Department of Energy's National Nuclear Security Administration under contract DE-AC04-94AL85000.

II. Load Mapping Methodology

The load mapping methodology is illustrated in Figure 1. Typically, blades are divided into multiple aerodynamic elements for computation of forces during the aeroelastic simulation. Aeroelastic simulation produces two forces and a moment for each blade element, and these loads are mapped to the individual nodes of the finite element model using the procedure shown below. Equations (1) through (3) define the necessary relationships between the blade element loads $\{F_x,F_y,M\}$ and the nodal loads $f_i(x,y)$ for a group of N nodes corresponding to the aeroelastic blade element. The reference location (x_r,y_r) is the point about which the aerodynamic moment is calculated.

$$F_x = \sum_{i=1}^{N} f_{x,i} \tag{1}$$

$$F_y = \sum_{i=1}^{N} f_{y,i} \tag{2}$$

$$M = \sum_{i=1}^{N} (x_i - x_r) \cdot f_{y,i} - (y_i - y_r) \cdot f_{x,i} \tag{3}$$

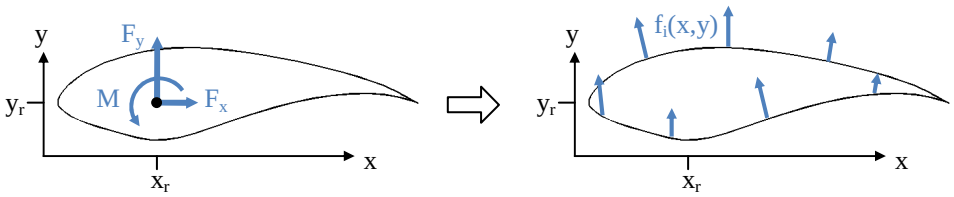

Figure 1. Illustration of load mapping procedure for a blade section.

The solution to the mapping problem is not unique, that is, there are many force distributions which produce the same resultant sectional loads. Therefore, a relationship between the node location (x_i,y_i) and f_i must be assumed. Equations (4) and (5) define linear spatial distributions for each force component.

$$f_{x,i} = a_x(y_i - y_r) + b_x \tag{4}$$

$$f_{y,i} = a_y(x_i - x_r) + b_y \tag{5}$$

Solution to the mapping problem is obtained by substituting Eqs. (4) and (5) into Eqs. (1)-(3). However, there are four unknown coefficients from the spatial distribution equations and only three resulting equations. This situation can be remedied either by reducing Eq. (4) to a constant rather than linear variation or by splitting Eq. (3) into two equations. The latter approach was taken in this work with the assumption that the x-direction forces produce zero moment. Equation (6) gives the matrix form of the resulting equations which can be solved using linear algebra.

$$\begin{bmatrix} m_y & 1 & 0 & 0 \\ 0 & 0 & m_x & 1 \\ 0 & 0 & m_{xx} & m_x \\ -m_{yy} & -m_y & 0 & 0 \end{bmatrix} \begin{Bmatrix} a_x \\ b_x \\ a_y \\ b_y \end{Bmatrix} = \begin{bmatrix} F_x/N \\ F_y/N \\ M/N \\ 0 \end{bmatrix} \tag{6}$$

where

$$m_x = \text{mean}(x_i - x_r)$$
$$m_y = \text{mean}(y_i - y_r)$$
$$m_{xx} = \text{mean}((x_i - x_r)^2)$$
$$m_{yy} = \text{mean}((y_i - y_r)^2)$$

III. Comparison to Pressure Distribution

The pressure distribution on an airfoil is more complex than the results captured by the load mapping technique previously discussed. Figure 2 illustrates a typical pressure distribution plot. Pressure distributions at various angles of attack were taken from Ref. 4 and converted to surface forces on the S825 airfoil outline. Then, the resultant

section loads $\{F_x,F_y,M\}$ were fed through the mapping procedure to obtain the mapped version of the surface forces. The force distributions are compared in Figure 3. Although some detail is missing from the mapped loading, the equivalent sectional forces and moment are the same and the localized differences should contribute very little to the overall structural response.

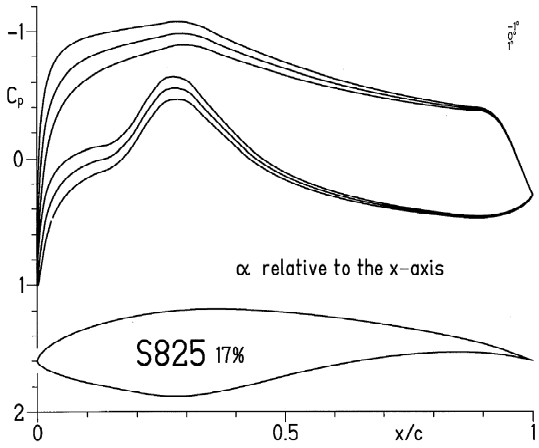

Figure 2. Pressure distribution of S825 airfoil near zero degrees angle of attack.[4]

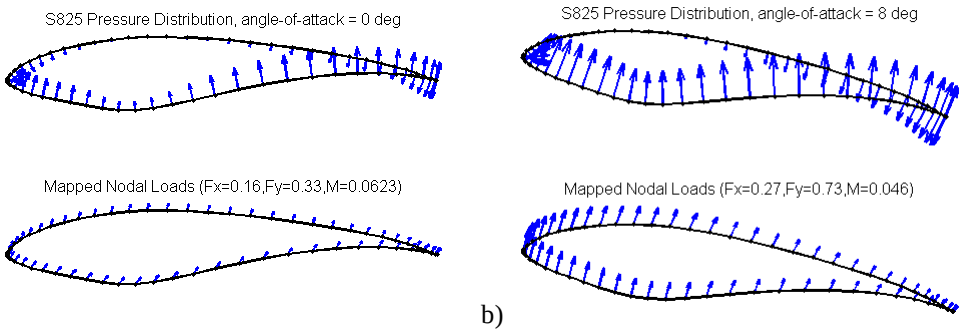

Figure 3. Comparison of pressure distribution (top) to the equivalent mapped loads using the technique discussed (bottom) at angle-of-attack a) 0 deg and b) 8 deg

IV. Eigen Buckling Analysis

This section presents the results of linear buckling analysis performed on a 1.5MW turbine blade FE model with loads applied using three approaches. The first approach applies a line of forces to the suction-surface spar cap using only the y-component of the one-dimensional beam loads. The second approach applies the same line of forces to the spar cap and also applies a line of forces to the leading edge using the x-component of the one-dimensional beam loads. The third approach utilizes the mapping technique discussed above to apply forces to every node in the FE model. The first and second approaches are examples of what a designer may choose to do if a more involved mapping technique is not readily available. The third approach requires more initial setup, but more closely represents the combined rotor normal, tangential, and blade torsion forces. A goal of this investigation is to learn about potential advantages of the more realistic load application approach. The one-dimensional beam loads are taken from a FAST[5] simulation of the "WP 1.5MW Baseline" model at the rated wind speed of 12 m/s.

Sandia National Laboratories has produced a NuMAD[6] model of the WindPACT 1.5MW blade design. Composite material stacks and blade geometry are defined according to publicly available literature[4,7-9]. The ANSYS mesh consisting of 5,178 SHELL281 elements (14966 nodes) is shown in Figure 4 with the low-pressure surface facing upward. Each colored area represents a different composite stack.

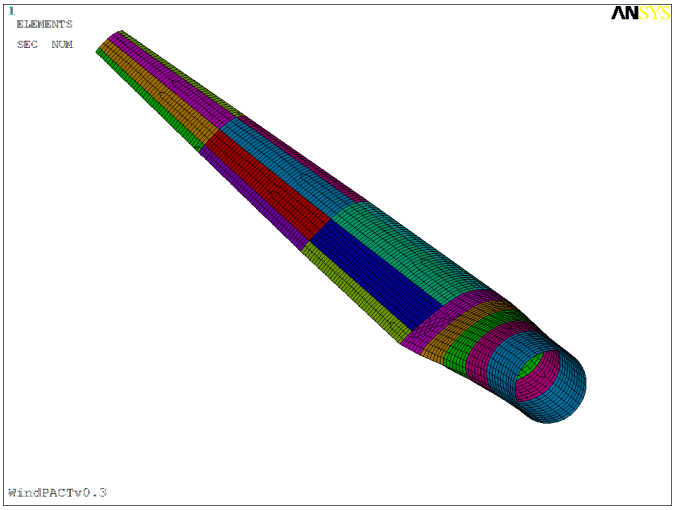

Figure 4. NuMAD-generated model of the WindPACT 1.5MW blade.

After meshing the model, the next step is to obtain a list of surface nodes for subsequent application of forces. In a typical NuMAD model, the elements with section numbers less than 1000 are skin elements and those with section number greater than 1000 are shear web elements. These statements are true as long as the section numbers have not been merged and compressed down. The blade skin nodes can be chosen by selecting the skin elements by the Section ID number attribute (ANSYS command "ESEL,S,SEC,,1,999") and then selecting all nodes associated with these elements ("ALLSEL,BELOW,ELEM"). A list of the selected nodes can be generated from the ANSYS List menu or by issuing the command "NLIST,ALL,,,XYZ,NODE".

A MATLAB script was written to take the list of nodes and apply the forces obtained from the FAST simulation. The FAST model is configured to output blade element data for each AeroDyn element. The script transforms forces normal and tangent to the rotor disk into flapwise and edgewise blade loads. Having defined a set of flapwise and edgewise loads from the one-dimensional beam, these loads are then mapped onto the FEM nodes with the following steps:

1. Divide the FEM nodes into spanwise groups corresponding to each element of the one-dimensional beam as defined in AeroDyn input file
2. For each group of nodes, use the above load mapping procedure to define forces for each node such that the resultant forces and moment in the x-y plane match the original element load.
3. Write an ANSYS batch file that creates the forces at each node ("F,*node*,[FX | FY],*magnitude*")

The second and third loading approaches applied to the blade are displayed in Figure 5.

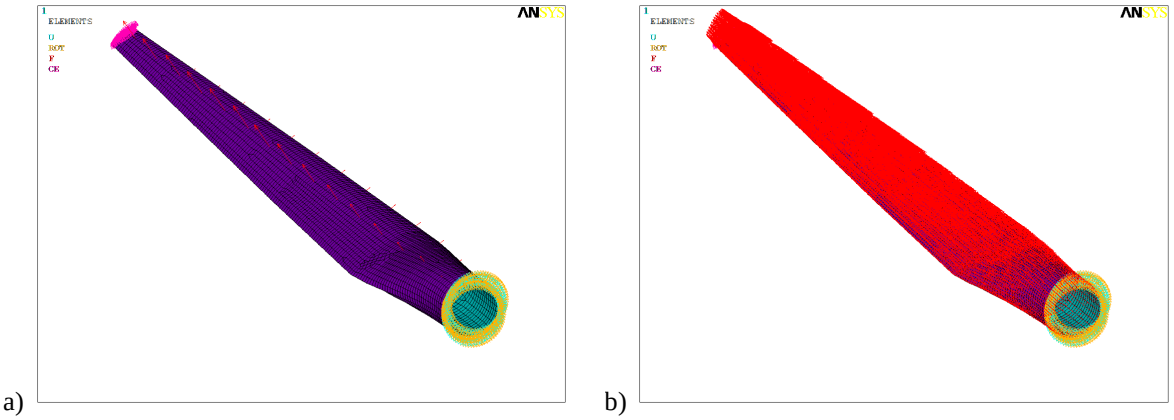

Figure 5. a) Line of forces on suction-surface spar and leading edge. b) Forces distributed among all nodes.

The first step in the eigenvalue buckling analysis is to run a Static analysis with Prestress Effects turned on. This option causes the applied load to modify the stiffness matrix in preparation for the buckling analysis. The next step is to choose an Eigen Buckling analysis. In this work, the Block Lanczos solver is utilized to find 20 buckling modes.

The results summary lists the load multiplier for each buckling mode. If the load multiplier is less than 1.0 then the structure is likely to fail under the applied load. If the load multiplier is greater than 1.0 then its value indicates how much the load magnitude can increase before buckling ensues. Table 1 lists the results summary for all three load cases. Mode shapes which appear to be valid buckling results have been numbered. The other results appear to be spurious buckling solutions (in which a few nodes have large displacements) which may have resulted from abrupt changes in shell thickness or other geometric problems within the blade model. Although the result set numbers differ, the buckling shapes correlate well between the loading approaches. Figures 6 and 7 illustrate the close correspondence of the first two buckling shapes. The load multipliers differ by 1.2% for both the first and second buckling modes. Load multipliers of modes three through six all differ by less than 1%.

One major difference observed between the two loading methods is the number of spurious buckling results and the presence of irregularities in some real modes. Applying loads as a line of forces on the spar cap tends to result in more spurious modes. For the most part, these spurious modes involve trailing edge nodes around max chord in the vicinity of material stack changes.

SET	Spar Force Line LOAD MULTIPLIER	Spar and L.E. Force Lines LOAD MULTIPLIER	Nodal Forces LOAD MULTIPLIER
1	0.75634	1.0741	1.0145
2	0.96211	1.4036	1.3384
3	1.2193	1.7167 (1st)	1.6605
4	1.4811	1.7583	1.7104 (1st)
5	1.6202	1.8807 (2nd)	1.8594
6	1.6908 (1st)	1.9619 (3rd?)	1.8916 (2nd)
7	1.7315	1.9888	1.9824 (3rd)
8	1.8183	2.1684 (4th)	2.1667 (4th)
9	1.9033	2.2161 (5th)	2.2166 (5th)
10	1.9147 (2nd)	2.2662 (6th)	2.2665 (6th)
11	1.9695 (3rd?)	2.3698 (7th)	2.3697 (7th)
12	1.9994	2.4448 (8th)	2.4397 (8th)
13	2.0468	2.4676 (9th)	2.4673 (9th)
14	2.1256	2.5834 (10th)	2.4970
15	2.1838 (4th)	2.6168	2.5605
16	2.2086	2.6643	2.5855 (10th)
17	2.2251 (5th)	2.6937	2.6023
18	2.2732 (6th?)	2.8206 (12th)	2.6297
19	2.3016	2.8516	2.6800 (11th)
20	2.3727	2.9312	2.8215 (12th)

Table 1. Results summary from linear buckling analysis for the two loading methods. Correspondence of similar buckling mode shapes has been identified.

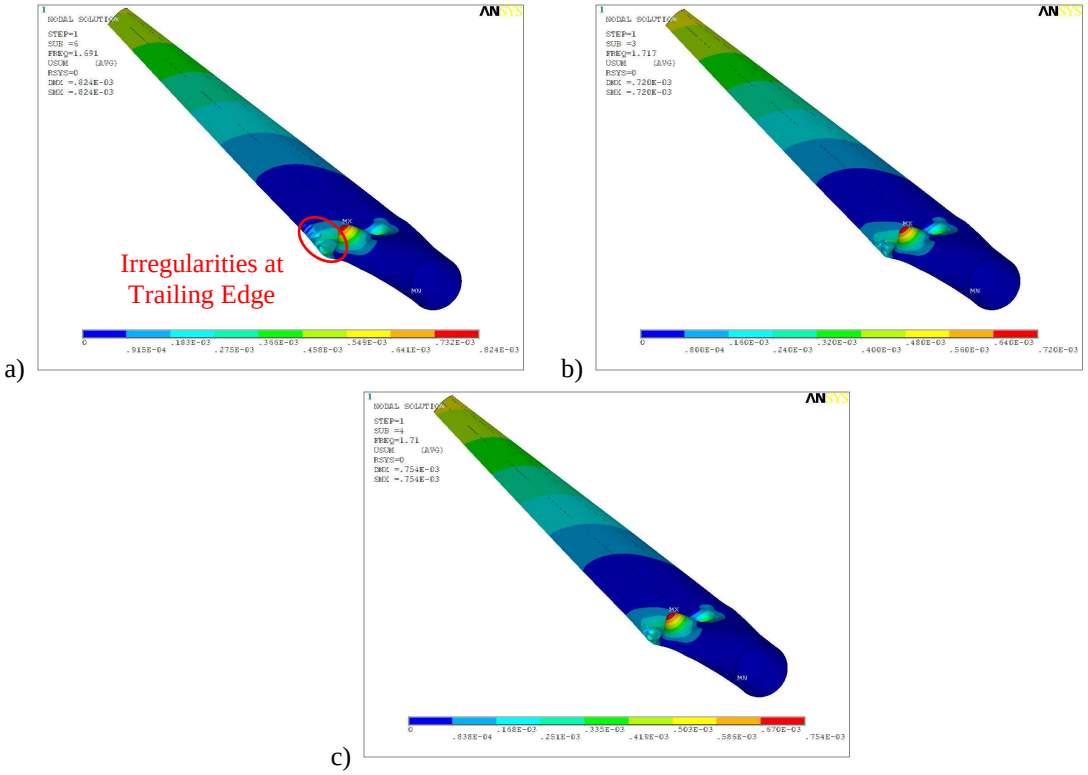

Figure 6. First buckling shape for a) spar line-load b) spar & L.E. line-loads and c) nodal-loads. Shapes correlate well, but the spar line-load model is sensitive to the trailinge edge geometry.

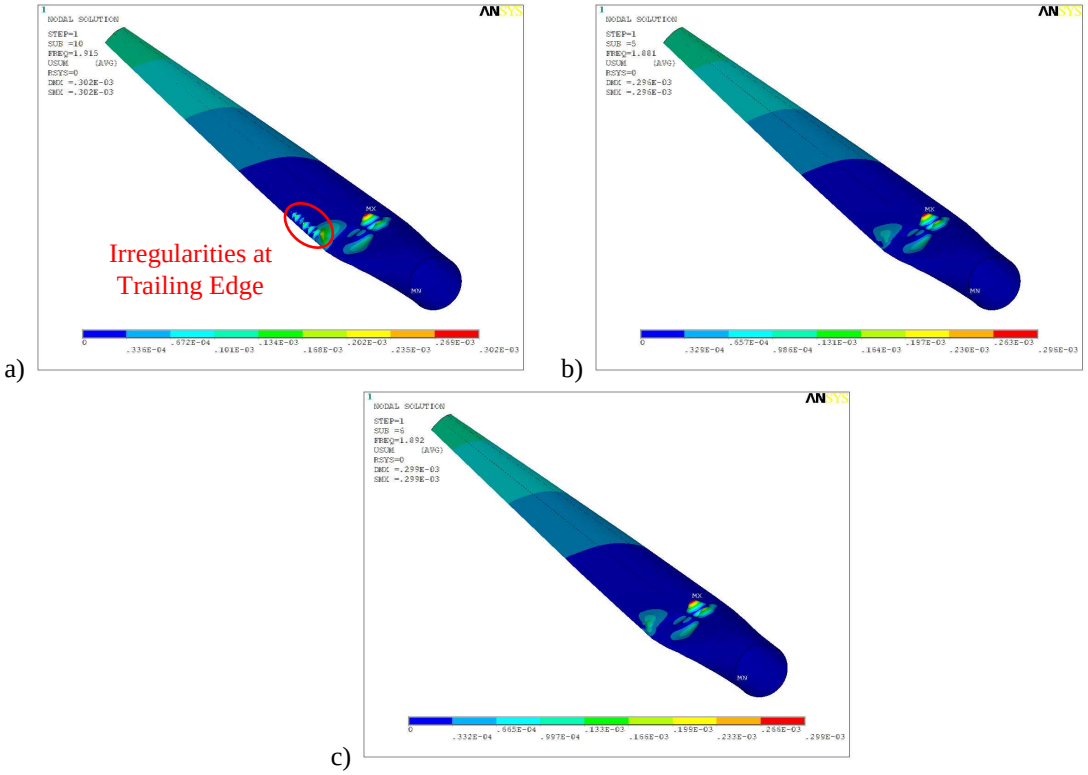

Figure 7. Second buckling shape for a) spar line-load b) spar & L.E. line-loads and c) nodal-loads. Shapes correlate well, but the spar line-load model is sensitive to the trailinge edge geometry.

V. Non-Linear Buckling Analysis

As linear buckling analyses can be non-conservative, a finite element analysis using non-linear displacement was also performed for a model loaded with point loads along the spar and another with linearly distributed loading. For this analysis, four-node SHELL181 elements were used with half the element edge length of the 8-node SHELL281 elements used in the previous analysis. The resulting model contained slightly more nodes (18842) than the previous model.

The deflected shape was first obtained from a linear buckling analysis which included pre-stress effects. The initial geometry was then perturbed by multiplying the deflected shape by the appropriate factor to achieve a series of imperfection amplitudes: 10 mm, 20 mm, and 50 mm. The model was then loaded until non-convergence occurred. The final deformed shapes for the two models are shown in Figure 8 and can be seen to be approximately the same. The resulting maximum load multiplier values for the two loading scenarios and imperfection sizes are shown in Table 2.

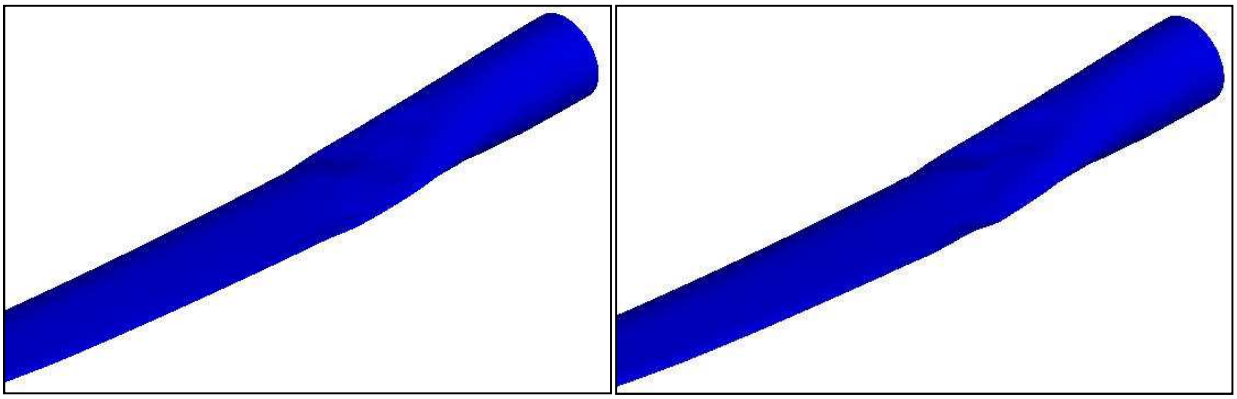

Figure 8. Deformed shapes obtained from non-linear analysis of model with spar-loading (left) and distributed loading (right) for an imperfection size of 20 mm.

Imperfection Size	Spar and L.E. Force Lines LOAD MULTIPLIER	Nodal Forces LOAD MULTIPLIER
10 mm	2.08	2.28
20 mm	2.00	2.19
50 mm	1.93	2.17

Table 2. Load multiplier values from non-linear analysis with a series of imperfection amplitudes.

The results point out two important considerations. First, the load multipliers in both cases are higher than the linear buckling analysis predicted which is counter to the typical non-conservative nature of these analyses. This indicates that the chosen buckled shape and associated load may not have been the most realistic for this blade and that a higher one should have been chosen instead. Second, the effect of distributing the forces over a larger set of nodes can be seen in the form of higher load multipliers for the distributed case. Loading at fewer points results in using higher loads and thus producing out-of-plane deflections which agrevate buckling and which are not realistic in actual operation.

VI. Conclusion

A technique for mapping one-dimensional beam loads from low-order aeroelastic simulation has been presented and a comparison was made between simple line loads and mapped nodal loads. In eigen buckling analysis, sensitivity to the trailing edge mesh geometry was observed when only flapwise loads were applied. However, when loads were applied in both the edge and flap directions, the line loads and mapped nodal loads produced very similar results. The mapped loading approach does appear to show a benefit in non-linear buckling analysis due to the greater sensitivity of non-linear analysis to deformed shape. Overall, the calculated buckling load for this blade model is relatively insensitive to the method of force application.

We intend to use analysis such as this to improve the realism of the WindPACT 1.5MW finite element model. The model is a useful demonstration model for utility scale blades and it will be used in future exercises. The current model is representative of the WindPACT concept, but analyses such as have been performed here point to a need for an even more realistic model, e.g. modeling of proper ply transistions and panel designs near maximum chord.

In previous blade design studies, spurious buckling modes such as were observed in this study were observed infrequently. As turbine blades grow to very large sizes, panel buckling becomes a governing design load case. It is critical that more time is spent understanding the cause of spurious buckling modes in the models. Additionally, sensitivity and uncertainty studies of parameters that govern buckling may prove to be useful.

The aeroelastic loads used in this investigation were for a relatively steady operational case - normal power generation. Some design load cases are due to transient environments in which the inertia of the blade will generate additional forces. Future load mapping techniques can incorporate these effects.

Finally, it will be useful to compare this load mapping technique to a direct pressure mapping of full rotor CFD pressures. The goal would be to understand where CFD pressures offer advantages in simulations realism over what is available using the simplified approach shown here. The rather meager differences observed in the present work between line loading and mapped distributed loading suggest that the use of CFD pressures may not offer a huge benefit. Setup and processing of a full rotor CFD problem requires extra time and effort compared to aeroelastic simulations that use beams and theories such as blade element momentum for aerodynamic rotor loads. Future work may determine what the benefits of a high fidelity CFD solution may offer over current, simplified approaches.

Acknowledgments

The authors acknowledge Tyler Bushnell for his contributions to the Sandia WindPACT 1.5MW NuMAD model.

References

[1] Bushnell, D., "Buckling of Shells—Pitfalls for Designers," *AIAA Journal*, Vol. 19, No. 9, 1981, pp. 1183-1226.

[2] McKittrick, L. R., Cairns, D. S., Mandell, J. F., Combs, D. C., Rabern, D. A., and VanLuchene R. D., "Analysis of a Composite Blade Design for the AOC 15/50 Wind Turbine Using a Finite Element Model," SAND2001-1441, May 2001. Albuquerque, NM USA: Sandia National Laboratories.

[3] Liu, W., Ma, Y., Su, X., and Huang, K., "Buckling Analysis of Wind Turbine Blade Using Pressure Distributions Obtained from CFD," *Power and Energy Engineering Conference*, APPEEC, 2009.

[4] Somers, D.M., "The S825 and S826 Airfoils," NREL Contractor Report NREL/SR-500-36344, January 2005.

[5] *NWTC Design Codes (FAST by Jason Jonkman, Ph.D.)*. http://wind.nrel.gov/designcodes/simulators/fast/. Last modified 05-November-2010; accessed 05-November-2010.

[6] Laird, D., Numerical Manufacturing And Design Tool (NuMAD by Daniel Laird), v2010.03.31. 2010.

[7] Griffin, D., "WindPACT Turbine Design Scaling Studies Technical Area 1.Composite Blades for 80- to 120-Meter Rotor. April 2001, NREL/SR-500-29492.

[8] Malcolm, D.J. and Hansen, A.C., "WindPACT Turbine Rotor Design Study," April 2006, NREL/SR-500-32495

[9] Somers, D. M., "The S816, S817, and S818 Airfoils," NREL Contractor Report NREL/SR-500-36333, December 2004.